Title
Selective Adsorption of Oxygen from Humid Air in a Metal—Organic Framework with Trigonal Pyramidal Copper(I) Sites

Journal
Journal of the American Chemical Society, 146(5)

ISSN
0002-7863

Authors
Carsch, Kurtis M
Huang, Adrian J
Dods, Matthew N
et al.

Publication Date
2024-02-07

DOI
10.1021/jacs.3c10753

Peer reviewed

JACS
JOURNAL OF THE AMERICAN CHEMICAL SOCIETY
pubs.acs.org/JACS

Article

Selective Adsorption of Oxygen from Humid Air in a Metal–Organic Framework with Trigonal Pyramidal Copper(I) Sites

Kurtis M. Carsch, Adrian J. Huang, Matthew N. Dods, Surya T. Parker, Rachel C. Rohde, Henry Z. H. Jiang, Yuto Yabuuchi, Sarah L. Karstens, Hyunchul Kwon, Romit Chakraborty, Karen C. Bustillo, Katie R. Meihaus, Hiroyasu Furukawa, Andrew M. Minor, Martin Head-Gordon, and Jeffrey R. Long*

Cite This: *J. Am. Chem. Soc.* 2024, 146, 3160–3170

Read Online

ACCESS | Metrics & More | Article Recommendations | Supporting Information

ABSTRACT: High or enriched-purity O_2 is used in numerous industries and is predominantly produced from the cryogenic distillation of air, an extremely capital- and energy-intensive process. There is significant interest in the development of new approaches for O_2-selective air separations, including the use of metal–organic frameworks featuring coordinatively unsaturated metal sites that can selectively bind O_2 over N_2 *via* electron transfer. However, most of these materials exhibit appreciable and/or reversible O_2 uptake only at low temperatures, and their open metal sites are also potential strong binding sites for the water present in air. Here, we study the framework Cu^I-MFU-4*l* ($Cu_xZn_{5-x}Cl_{4-x}(btdd)_3$; H_2btdd = bis(1*H*-1,2,3-triazolo[4,5-*b*],[4′,5′-*i*])dibenzo[1,4]dioxin), which binds O_2 reversibly at ambient temperature. We develop an optimized synthesis for the material to access a high density of trigonal pyramidal Cu^I sites, and we show that this material reversibly captures O_2 from air at 25 °C, even in the presence of water. When exposed to air up to 100% relative humidity, Cu^I-MFU-4*l* retains a constant O_2 capacity over the course of repeated cycling under dynamic breakthrough conditions. While this material simultaneously adsorbs N_2, differences in O_2 and N_2 desorption kinetics allow for the isolation of high-purity O_2 (>99%) under relatively mild regeneration conditions. Spectroscopic, magnetic, and computational analyses reveal that O_2 binds to the copper(I) sites to form copper(II)–superoxide moieties that exhibit temperature-dependent side-on and end-on binding modes. Overall, these results suggest that Cu^I-MFU-4*l* is a promising material for the separation of O_2 from ambient air, even without dehumidification.

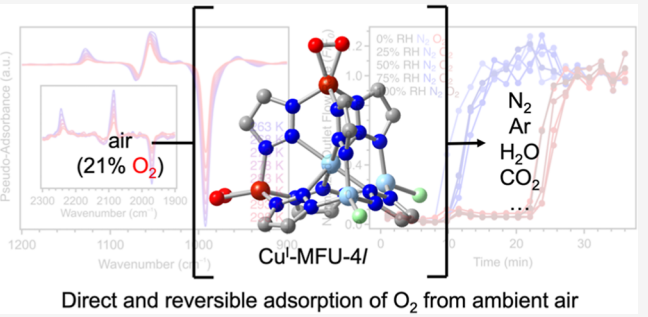

Direct and reversible adsorption of O_2 from ambient air

INTRODUCTION

Enriched- or high-purity O_2 is a critical commodity in the medical, manufacturing, and aerospace industries and for the production of feedstock chemicals such as ethylene oxide and phthalic anhydride.[1,2] The vast majority of O_2 is produced from the cryogenic distillation of air.[3,4] This energy-intensive, multistep process involves the compression and pretreatment of air to remove volatile organic compounds, water, and CO_2, and then the resulting gaseous mixture—predominantly O_2, N_2, and Ar is expanded and cooled to cryogenic temperatures upon passing through a series of heat exchangers, before being fed into distillation columns where O_2 is separated from N_2 and Ar. A simplified illustration of the basic steps required for the cryogenic distillation of air is shown in Figure 1a. Ultimately, while cryogenic distillation is the most mature and widely used technology for air separations, there is significant interest in identifying more energy-efficient and scalable methods for isolating O_2 from air.

The prospect of using O_2-selective adsorbents for energy-efficient air separations has garnered research attention for decades,[4,5] beginning with early studies of O_2 binding in molecular cobalt(II) complexes.[6] A renaissance in this area has occurred within the previous decade with the discovery that certain porous, microcrystalline metal–organic frameworks (MOFs) featuring coordinatively unsaturated iron(II),[7−9] cobalt(II),[10−13] and chromium(II)[14,15] sites can bind O_2 *via* electron transfer mechanisms that give rise to excellent selectivities for O_2 over typically redox-inactive N_2. The reader is referred to two recent perspective articles published on this topic.[4,16] Importantly, air separations using cation-exchanged zeolites that selectively adsorb N_2 over O_2 (and Ar) are already used in industry to supplement cryogenic distillation for

Received: September 28, 2023
Revised: January 7, 2024
Accepted: January 8, 2024
Published: January 26, 2024

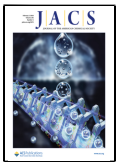

https://doi.org/10.1021/jacs.3c10753
J. Am. Chem. Soc. 2024, 146, 3160–3170

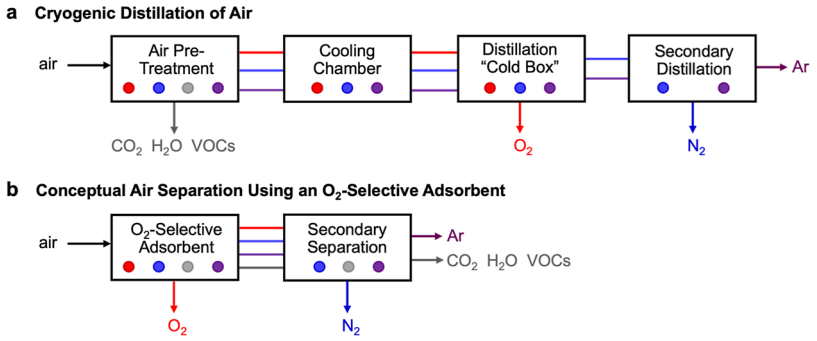

Figure 1. (a) Simplified process flow diagram of current industrial air separation, entailing air pretreatment to remove condensable volatiles, followed by cryogenic distillation to isolate O_2. Note that the initial pretreatment step often entails adsorption along with its associated unit operations, which are not shown in detail here. A subsequent secondary distillation is used to separate N_2 and Ar. VOC denotes volatile organic compounds, which present safety issues due to potential uncontrolled oxidations with liquid oxygen in the distillation "cold box".[18,19] (b) More desirable adsorbent-based air separation would entail the direct removal of O_2 from untreated air at ambient temperatures, followed by secondary separation to purify N_2 and Ar.

applications where O_2 purities <95% are sufficient (*e.g.*, for medicinal use). As such, in particular for medium to small-scale applications, infrastructure is in place that could in principle be adapted to implement separations technology using O_2-selective adsorbents[3,4]

A porous adsorbent capable of selectively capturing O_2 over N_2 and the other components of air, such as water, could be used to produce high purity O_2 from air in a process that requires no pretreatment[17] (other than removal of particulate matter) and is thus in principle operationally simpler than cryogenic distillation or N_2-selective adsorptive separations.[18,19] An illustration of such a hypothetical process is given in Figure 1b, although we note that this is a conceptual diagram only, intended to highlight an idealized process flow for such an adsorbent. In principle, far less adsorbent would be required to treat a given quantity of air in such a process than would be needed for an equivalent air separation using an N_2-selective zeolite, since the concentration of O_2 (21%) in air is much less than the concentration of N_2 (78%).[4] Consequently, the capital and energy expenditures required for air separations using an O_2-selective adsorbent could be significantly less than what is required for cryogenic distillation and current adsorptive separations.[4] However, the majority of O_2-selective MOFs studied to date adsorb appreciable O_2 only at subambient temperatures[7−13,20] or exhibit poor stability to repeated cycling.[14,15,21] Additionally, these materials feature coordinatively unsaturated, Lewis acidic metal sites that can also serve as strong binding sites for water.[22,23] Importantly, none of the corresponding studies has examined adsorbent O_2 selectivity and capacity in the presence of water vapor, which is a non-negligible component of air.

A noteworthy framework in the context of air separations is Cu^I-MFU-4*l* ($Cu_xZn_{5-x}(Cl/OOCH)_{4-x}(btdd)_3$; H_2btdd = bis(1*H*-1,2,3-triazolo[4,5-*b*],[4′,5′-*i*])dibenzo[1,4]dioxin), which features pentanuclear cluster nodes consisting of a central octahedral zinc(II) ion coordinated to four peripheral metal ions either pyramidal copper(I) or tetrahedral zinc(II) (Figure 2a,b). Under ambient conditions, the copper(I) sites in the framework have been shown to strongly and reversibly bind O_2,[24] and the favorable calculated ΔG° of O_2 binding at 298 K in this material suggests that it may be promising candidate for O_2-selective adsorptive air separations.[4] Additionally, in the context of hard−soft acid−base theory, we hypothesized that the intrinsic mismatch between the soft copper(I) ion and hard water molecule may render Cu^I-MFU-4*l* selective for O_2 even in the presence of water.[25]

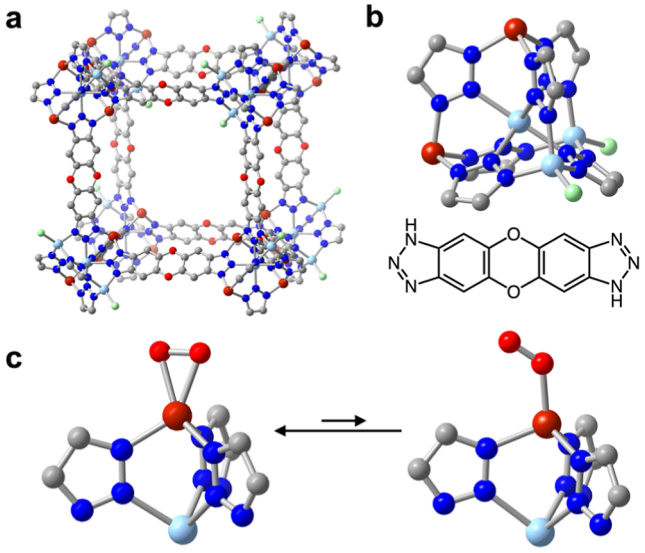

Figure 2. (a) Solid-state structure of $Cu_{2.4}$-MFU-4*l* determined from Rietveld refinement of synchrotron powder X-ray diffraction data (Figure S50). The framework $Cu_{2.4}$-MFU-4*l* was prepared *via* an optimized synthesis route involving the direct reaction of $Zn_5Cl_4(btdd)_3$ with copper(I) chloride dimethylsulfide. Note that the Cu and Zn sites are disordered such that the aggregate ratio of Cu to Zn is 2.4 to 2.6 for the framework. (b) (Upper) Expanded view of a pentanuclear node in $Cu_{2.4}$-MFU-4*l*. (Lower) Structure of the H_2btdd linker. (c) Illustration of calculated structures for superoxide bound in a side-on and end-on fashion to copper(II) sites in the model pentanuclear cluster $Cu_2Zn_3Cl_2(bta)_6$ (ta^- = 1,2,3-benzotriazolate; see the Supporting Information for details). Vibrational spectroscopy analysis supports that O_2 adsorbs in $Cu_{2.4}$-MFU-4*l* to generate both side-on and end-on superoxide bound to copper(II), which are in temperature-dependent equilibrium (Figure 3). Brown, light blue, green, red, dark blue, and gray spheres represent Cu, Zn, O, N, Cl, and C atoms, respectively.

Herein, we disclose that Cu^I-MFU-4*l*, synthesized with new optimized procedures that result in higher Cu^I loadings, is able to reversibly adsorb O_2 from air at ambient temperatures with excellent cyclability, even in the presence of water vapor. Variable-temperature *in situ* diffuse reflectance infrared Fourier transform spectroscopy (DRIFTS) and magnetic susceptibility

https://doi.org/10.1021/jacs.3c10753
J. Am. Chem. Soc. 2024, 146, 3160−3170

data indicate that O_2 binds at the copper(I) sites to form copper(II)−superoxide motifs and that side- and end-on superoxide binding modes are in equilibrium over a range of temperatures. We find that differences in the kinetics of desorption of O_2 and N_2 from the framework allow for the isolation of high-purity O_2, providing a new approach to separate O_2 directly from ambient air.

RESULTS AND DISCUSSION

Materials Synthesis and Characterization. The framework Cu^I-MFU-4*l* was initially synthesized following the literature protocol.[26] In brief, $Zn_5Cl_4(btdd)_3$ (MFU-4*l*)[24] was treated with excess $CuCl_2$ in *N*,*N*-dimethylacetamide under an inert atmosphere at 60 °C to give $Cu^{II}Cl$-MFU-4*l* [$Cu^{II}_{2.2}Zn_{2.8}Cl_4(btdd)_3$ based on inductively coupled plasma optical emission spectroscopy, ICP-OES]. Subsequent anion exchange with lithium formate monohydrate and thermolysis at 180 °C afforded Cu^I-MFU-4*l* (Figure S38). When prepared using this route, Cu^I-MFU-4*l* has been reported to contain a mixture of copper(I) and copper(II) ions.[27−29] The copper(I) sites in this material are known to strongly bind H_2,[24,26] and therefore as a means of qualitatively estimating the number of these sites in Cu^I-MFU-4*l*, we collected H_2 adsorption isotherms at 77 K and pressures ranging from 0 to 1.2 bar (Figure S7). The material exhibits steep H_2 uptake at low pressures and achieves a capacity of 1.3 mmol/g at 1 mbar, followed by more gradual uptake at higher pressures indicative of H_2 physisorption. If all of the copper sites in the material were trigonal pyramidal copper(I), and assuming a 1:1 stoichiometry for H_2 binding,[24] we would expect a low-pressure uptake of approximately 1.9 mmol/g (based on the copper site stoichiometry determined for the Cu^{II}-MFU-4*l* precursor from ICP-OES). From the measured uptake of 1.3 mmol/g at 1 mbar, we then estimate that ∼68% of the copper ions are exposed copper(I) sites.[30] While estimates of copper(I) loading achieved in this way are qualitative (see Figure S7), we propose that the H_2 uptake at 1 mbar may be a useful means of estimating and comparing copper(I) loading in Cu^I-MFU-4*l* materials [see Table S2 for a comparison of reported copper(I) loadings in various Cu^I-MFU-4*l* samples prepared in the literature and other qualitative approaches used to evaluate loadings].

With the goal of accessing a form of Cu^I-MFU-4*l* featuring a greater number of copper(I) sites per node and therefore higher gas adsorption capacities, we sought to optimize the synthesis of this material. For simplicity, we denote Cu^I-MFU-4*l* materials prepared *via* different routes simply as Cu_x-MFU-4*l*, where *x* specifies the total number Cu sites per node as quantified by ICP-OES analysis of the copper(II) precursor (*e.g.*, the shorthand for Cu^I-MFU-4*l* prepared *via* the literature route[24,26] is $Cu_{2.2}$-MFU-4*l*). Following extensive optimization, we found that treatment of $Zn_5Cl_4(btdd)_3$ with 40 equiv of $CuCl_2$ in anhydrous dimethyl sulfoxide at 60 °C yields a material with 2.7 Cu^{II} ions per pentanuclear node, based on energy-dispersive X-ray spectroscopy and ICP-OES (Figures S29 and S30). Two sequential additions of lithium formate monohydrate followed by a thermolysis sequence ending with heating at 250 °C afforded a material with the formula $Cu_{2.7}Zn_{2.3}H_{0.9}Cl_{0.7}(btdd)_3$ (hereafter, $Cu_{2.7}$-MFU-4*l*; see Section S2 of the Supporting Information for synthesis details and Figures S15, S29, S34, S37, and S38).

Analysis of H_2 adsorption data collected at 77 K revealed that $Cu_{2.7}$-MFU-4*l* adsorbs 2.1 mmol/g at 1 mbar of H_2, nearly double the capacity measured for $Cu_{2.2}$-MFU-4*l* under the same conditions (Figure S8; Table S2). From this uptake, we estimate that approximately 89% of the copper sites in the material are copper(I), which is one of the highest levels of copper(I) incorporation reported for Cu^I-MFU-4*l* to date. As validation of this approach, we also conducted an experiment where we dosed a tared sample of activated $Cu_{2.7}$-MFU-4*l* with 50 mbar of CO at 298 K to saturate the copper(I) sites[24] and then evacuated the sample to remove physisorbed CO. The resulting sample mass increased by 5.8(1) wt %, corresponding to a copper(I) loading of 2.4(1) per node, consistent with the copper(I) loading estimated from the H_2 adsorption data (see Table S14). Analysis of 77 K N_2 adsorption data revealed that $Cu_{2.7}$-MFU-4*l* has a high BET surface area of 4160(40) m^2/g (Figure S1) that exceeds previously reported values for Cu^I-MFU-4*l* (347−4000 m^2/g, see Table S2).[24,26,28,31−34] Thermal decomposition profiles collected under dry N_2 and O_2 revealed that the material is stable until approximately 400 and 280 °C, respectively, under these gases (Figure S16). We found it is also possible to prepare Cu^I-MFU-4*l* *via* the abovementioned route using hydrated $CuCl_2$ in dimethyl sulfoxide without the exclusion of air or water (see Section S2 of the Supporting Information for details). The resulting material exhibits a similarly high H_2 capacity of 1.9 mmol/g at 77 K and 1 mbar (Figure S9).

In our optimization of the synthesis of Cu^I-MFU-4*l*, we also found that treatment of $Zn_5Cl_4(btdd)_3$ with copper(I) chloride dimethylsulfide in acetonitrile at 25 °C and activation of the resulting framework at 300 °C affords $Cu_{2.4}Zn_{2.6}Cl_{1.6}(btdd)_3$ ($Cu_{2.4}$-MFU-4*l*; see Figures 2a,b, S31, S35, and S36). The H_2 adsorption capacity measured for this material at 77 K and 1 mbar is 2.0 mmol/g, consistent with the theoretical capacity assuming binding of one molecule of H_2 per Cu(I) site in the material (2.0 mmol/g) (Figure S7; a consistent loading was also determined from analysis of CO uptake in the material, see Table S14). Advantageously, this approach affords access to Cu^I-MFU-4*l* with a more well-defined formula and in fewer synthetic steps than the materials accessed *via* copper(II) substitution and autoreduction. The BET surface area of $Cu_{2.4}$-MFU-4*l* is 3820(30) m^2/g (Figure S1), which is slightly lower than the surface area measured for $Cu_{2.7}$-MFU-4*l* and consistent with the presence of only chloride capping ligands, in contrast to the mixture of chloride and smaller hydride ligands in $Cu_{2.7}$-MFU-4*l*. For all O_2, N_2, and Ar isotherm data collection (see below), we employed $Cu_{2.7}$-MFU-4*l* based on its slightly higher estimated copper(I) loading, while $Cu_{2.4}$-MFU-4*l* was used for spectroscopic analyses due to its greater homogeneity of copper ions and coordinated anions.[35]

Structural, Spectroscopic, and Computational Characterization of O_2 Binding. As noted above, Cu^I-MFU-4*l* is known to reversibly bind O_2 at room temperature,[24] and a recent investigation of O_2 binding in Cu^I-MFU-4*l* using *in situ* Cu $L_{2,3}$-edge near-edge X-ray absorption fine structure spectroscopy and time-dependent density functional theory revealed that O_2 adsorption is accompanied by significant electron transfer from copper(I) to O_2 with partial oxidation of the copper ion.[27] We sought to better understand the nature of the binding of the binding of the O_2 species in this material using a suite of structural, spectroscopic, and computational analyses. Dosing microcrystalline $Cu_{2.4}$-MFU-4*l* with 8 mbar of O_2 at 195 K resulted in a rapid color change from off-white to pink, indicative of a change in the copper oxidation state. Analysis of powder X-ray diffraction data collected for $Cu_{2.4}$-

https://doi.org/10.1021/jacs.3c10753
J. Am. Chem. Soc. 2024, 146, 3160−3170

MFU-4*l* at 195 K before and after dosing with 8 mbar of O_2 revealed a shift in the peak positions to higher 2θ values with gas dosing, while dosing with higher O_2 pressures of 109 and 1005 mbar did not lead to further changes in the peak positions (Figure S45).

Pawley fits against the diffraction data for activated $Cu_{2.4}$-MFU-4*l* collected under vacuum and the sample dosed with 8 mbar of O_2 revealed a unit cell contraction upon O_2 binding from 31.2090(14) to 31.0044(3) Å (cubic space group $Fm\bar{3}m$, see Figures S42 and S43), while a smaller unit cell contraction was characterized upon dosing the material with 9 mbar of N_2 at 195 K [from 31.2090(14) to 31.0997(11) Å, Figure S44]. These results suggest a greater perturbation of the local electronic structure around the copper(I) ions upon O_2 binding *versus* N_2 binding, and the decrease in unit cell parameter upon O_2 dosing is consistent with the shortening of the metal−ligand bonds due to copper oxidation. Rietveld refinement of the diffraction data collected for activated $Cu_{2.4}$-MFU-4*l* revealed a structure consistent with that reported previously based on neutron powder diffraction data (Figure 2a,b).[26] Rietveld refinement of the diffraction data for O_2-dosed $Cu_{2.4}$-MFU-4*l* using the structure of the activated framework as a starting model revealed electron density above the copper sites that was refined as O_2, yielding an occupancy of 2.8(4) molecules per node (Figures S47 and S48). However, the structural disorder of the O_2 motif about the C_3 axis as well as the crystallographic superposition of the zinc and copper ions preclude meaningful commentary on structural metrics or the nature of O_2 binding.

We turned to variable-temperature *in situ* DRIFTS to further investigate the nature of the binding of O_2 in $Cu_{2.4}$-MFU-4*l*. Dosing the material with up to 1 bar of O_2 at 300 K resulted in clear changes in the fingerprint region (600 to 1400 cm^{-1}) (Figure S35). To elucidate the features arising from bound O_2, we conducted identical experiments in which $Cu_{2.4}$-MFU-4*l* was dosed at 263 K with 8 mbar of either natural abundance O_2 (99.8% $^{16}O_2$) or $^{18}O_2$ (97 atom % ^{18}O). Spectra were then collected at 5 K intervals as the sample was warmed from 263 to 298 K. A set of difference spectra generated by subtracting the $^{18}O_2$-dosed spectra from the O_2-dosed spectra are plotted in Figure 3a and clearly show positive and negative peaks corresponding to $^{16}O_2$ and $^{18}O_2$ vibrations, respectively. Intriguingly, two sets of features were generated upon O_2 dosing: one pair at 1131 and 1051 cm^{-1} and another pair at 1073 and 993 cm^{-1} for the O_2- and $^{18}O_2$-dosed samples, respectively. The isotopic shifts for both features are consistent with predictions based on the simple harmonic oscillator model for O_2 (peaks for $^{18}O_2$-dosed material are predicted to be at 1066 and 990 cm^{-1}). As such, we assign both sets of features to the O_2 species.

To determine the origins of these resonances, we performed another set of experiments in which the activated framework was dosed with either 45 mbar O_2 or $^{18}O_2$ at 300 K, cooled to 100 K to saturate the copper(I) sites, and then spectra were collected as the sample was incrementally warmed to room temperature (Figure 3b). Interestingly, a reversible color change from pink to gray-brown was observed upon warming the sample from 100 K to room temperature (Figure S61). At 100 K, only the peaks at 1051 and 993 cm^{-1} were present, while above 200 K, the peaks at 1131 and 1073 cm^{-1} were also apparent. We assign the lower energy features to a superoxide-bound side-on (η^2) to Cu^{II} (typically 970−1100 cm^{-1})[36−38] and the higher energy features to a superoxide-bound end-on (η^1) to Cu^{II} (typically 1100−1150 cm^{-1}).[38−41] Interestingly, this is to our knowledge the first example of a copper−O_2 adduct where the coordinated O_2 species exhibits a temperature-dependent equilibrium between binding modes. Dosing $Cu_{2.4}$-MFU-4*l* with air at room temperature results in an additional resonance at 2242 cm^{-1} associated with N_2 adsorption.[24] This resonance is red-shifted from the Raman active mode of free N_2 (2331 cm^{-1}),[42] indicating the copper(I) sites function as a weak π-donor for N_2.[27]

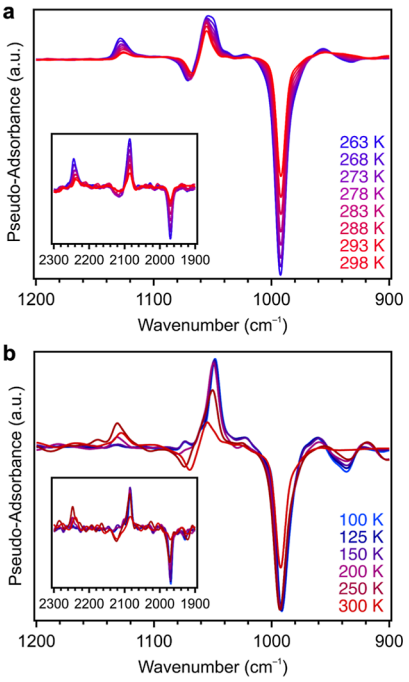

Figure 3. (a) Difference spectra obtained by subtracting DRIFTS data collected upon warming (263 to 298 K) a sample of $Cu_{2.4}$-MFU-4*l* dosed with O_2 from the corresponding data for $Cu_{2.4}$-MFU-4*l* dosed with $^{18}O_2$. (b) Difference spectra generated by subtracting DRIFTS data collected upon warming (100 to 300 K) a sample of $Cu_{2.4}$-MFU-4*l* dosed with $^{18}O_2$ (negative features) from the corresponding data for $Cu_{2.4}$-MFU-4*l* dosed with O_2 (positive features). Peaks corresponding to a secondary, less activated superoxide species appear at 200 K. The lower and higher energy features in both sets of spectra are assigned to superoxide species bound to copper(II) in a side-on and end-on fashion, respectively. Insets depict superoxide overtones.

The spin state of a copper−O_2 adduct depends on the O_2 binding mode. In particular, η^2-O_2 adducts have been found to possess a singlet ground state ($S = 0$),[38,43] while η^1-O_2 adducts possess a triplet ground state ($S = 1$).[38,44] As such, to support the assignments made based on the *in situ* DRIFTS data, variable-temperature dc magnetic susceptibility data were collected at 1 T for a sample of $Cu_{2.4}$-MFU-4*l* dosed with O_2 at 195 K (see the Supporting Information for details and Figures S49 and S50). Below 195 K, the magnitude of the molar magnetic susceptibility−temperature product ($\chi_M T$) is close to zero. However, as the material is warmed above 200 K, $\chi_M T$ steadily increases to 0.25 emu·K/mol. Although the values of $\chi_M T$ should be treated qualitatively due to challenges with the sample diamagnetic correction and desorption of O_2 at higher temperatures, these data are consistent with an equilibrium between the $S = 0$ and $S = 1$ species, in which the higher spin state is at least partially accessed upon warming.

https://doi.org/10.1021/jacs.3c10753
J. Am. Chem. Soc. 2024, 146, 3160−3170

Density functional theory (DFT) calculations carried out on a pentanuclear cluster model of Cu^{I}-MFU-4*l* further support an equilibrium between the O_2 bound side-on and end-on to the copper sites in the framework (see Section S10 of the Supporting Information and Figure 2c). In particular, the η^2-O_2 binding mode was found to be favored based on electronic energies over the η^1-O_2 binding mode (ΔE = −65 *versus* −46 kJ mol^{-1}, respectively). Additionally, the calculated O−O bond lengths for O_2 bound in an η^2 and η^1 fashion are slightly longer than the O−O bond length for gaseous O_2 (calculated 1.31 and 1.26 Å for O_2 *versus* 1.21 Å, respectively), consistent with electron transfer from copper(I) to O_2 to form a copper(II)−superoxo ($O_2^{\bullet-}$) moiety. Taken together, the structural, spectroscopic, and computational results support the formation of Cu^{II}−$O_2^{\bullet-}$ moieties upon O_2 binding in Cu^{I}-MFU-4*l*.[45]

Investigation of O_2, N_2, Ar, and H_2O Adsorption. Single-component O_2, N_2, and Ar isotherms were collected for $Cu_{2.7}$-MFU-4*l* at 298 K and pressures ranging from 0 to 1 bar (Figure 4a). Consistent with binding of the O_2 at the open copper sites, the material exhibits relatively steep uptake of the O_2 at low pressures and achieves a capacity of 1.5 mmol/g at 210 mbar, the partial pressure of the O_2 in air. This is the second highest O_2 capacity reported for a MOF under these conditions (see Table S3), exceeded only by $Cr_3[(Cr_4Cl)_3(BTT)_8]_2$ (Cr-BTT; BTT^{3-} = 1,3,5-benzenetris-tetrazolate), which exhibits a capacity of 2.2 mmol/g.[15] However, Cr-BTT is not stable for repeated cycling with O_2 under conditions relevant to uptake from ambient air, unlike $Cu_{2.7}$-MFU-4*l* (see below). Oxygen uptake in $Cu_{2.7}$-MFU-4*l* begins to level off at higher pressures, reaching a value of 2.0 mmol/g at 1 bar O_2. Assuming that one O_2 molecule binds at every copper(I) site, the theoretical capacity (excluding adsorption at secondary sites in the material) is 2.1 mmol/g. Considering that the capacity at 1 bar represents both chemisorption and physisorption, the experimental uptake suggests that not all copper(I) sites in this framework are saturated at this pressure. Nitrogen uptake in $Cu_{2.7}$-MFU-4*l* is more gradual at low pressures, and the material adsorbs less N_2 than does O_2 over the entire pressure range (1.5 mmol/g at 1 bar). However, at the partial pressure of N_2 in air (780 mbar), the material exhibits a N_2 capacity of 1.3 mmol/g N_2 that is only slightly less than the O_2 capacity at 210 mbar. Finally, $Cu_{2.7}$-MFU-4*l* adsorbs very little Ar at 298 K between 0 and 1 bar, and at 9 mbar, the partial pressure of Ar in air, the material adsorbs <0.01 mmol/g.

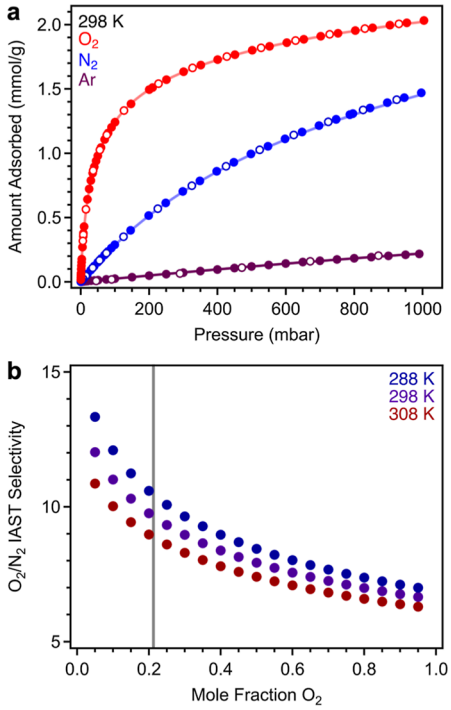

Figure 4. (a) Single-component O_2, N_2, and Ar adsorption (filled circles) and desorption (open circles) isotherm data collected at 298 K for $Cu_{2.7}$-MFU-4*l*. Colored lines represent calculated curves obtained from simultaneous fitting of three single-component isotherms at different temperatures with either a dual-site Langmuir−Freundlich equation (N_2, O_2: 288, 298, and 308 K) or a single Langmuir−Freundlich equation (Ar: 170, 180, and 190 K). (b) Variable-temperature IAST selectivities calculated for a binary O_2/N_2 mixture. The O_2 concentration in air (21%) is denoted with a vertical gray line.

Variable-temperature Ar, O_2, and N_2 adsorption isotherms were collected to determine the enthalpies of adsorption in $Cu_{2.7}$-MFU-4*l* (Figures S5 and S6). Low-temperature Ar isotherms were collected at 170, 180, and 190 K, and these data could be simultaneously modeled using the single-site Langmuir−Freundlich equation (Figure S6). In contrast, a dual-site Langmuir−Freundlich equation was needed to model O_2 and N_2 isotherms collected at 288, 298, and 308 K, consistent with primary gas binding at the copper sites and secondary interactions with the framework (Table S4). Using the fits to these data and the Clausius−Clapeyron equation, we determined O_2, N_2, and Ar adsorption enthalpies as a function of loading (Figure S13). The isosteric enthalpy of adsorption (ΔH_{ads}) at low loadings of O_2 is −56.8(1) kJ/mol, higher than the values determined for N_2 [−38.9(4) kJ/mol] and Ar [−10.9(1) kJ/mol]. The enthalpy of Ar adsorption is consistent with weak adsorbate−framework interactions[46] and remains essentially constant with loading, while the heats of adsorption for O_2 and N_2 gradually decline as the copper sites become saturated and secondary adsorption sites within the framework are occupied. The O_2 and N_2 adsorption enthalpies are consistent with previously reported isosteric enthalpy (heat) of adsorption in Cu^{I}-MFU-4*l* [$\Delta H_{ads} = -Q_{st}$ = −52.6(6) and −41.6(6) kJ/mol, respectively; see Table S3 for heats of O_2 and N_2 adsorption reported for other relevant frameworks][24] and indicative of strong interactions with the open copper(I) sites. This result is consistent with the DRIFTS data and the electron transfer from copper(I) to O_2.

Ideal adsorption solution theory (IAST)[47] was used to predict the equilibrium adsorption behavior of $Cu_{2.7}$-MFU-4*l* exposed to a binary O_2/N_2 mixture and extract O_2/N_2 adsorption selectivities as a function of O_2 concentration (see the Supporting Information for details). For a binary mixture containing 21% O_2, the O_2/N_2 selectivity is 10 at 298 K, which would correspond to 72% adsorbed phase purity (74% at 288 K; Figure 4b). However, it should be noted that one of the assumptions of IAST is that there is a homogeneous distribution of guests within the pores of the material,[48] an assumption that is not likely to hold for Cu^{I}-MFU-4*l*, where electron transfer is a driving force in O_2 binding but not in the case of N_2 binding. In a realistic scenario where O_2 preferentially clusters around the copper(I) sites, IAST is expected to overestimate actual selectivity values.[48] However, breakthrough analysis using dry and humid compressed air streams indicates that O_2 does indeed bind selectively over N_2

https://doi.org/10.1021/jacs.3c10753
J. Am. Chem. Soc. 2024, 146, 3160−3170

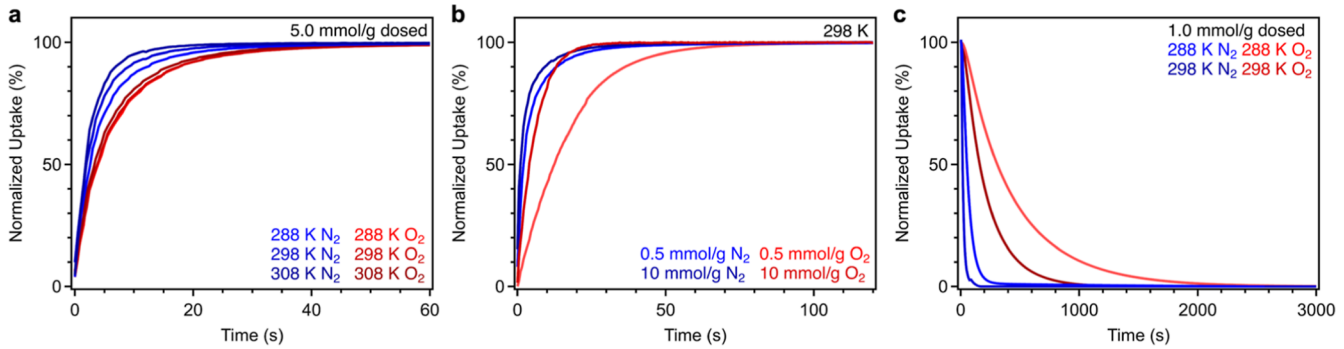

Figure 5. (a) Normalized adsorption kinetic traces for $Cu_{2.7}$-MFU-4*l* dosed with 5.0 mmol/g N_2 and O_2 at 288, 298, and 308 K. Nitrogen adsorption and equilibrium in the material occurs slightly more rapidly than for O_2 at all temperatures. (b) Higher initial dosing quantity for N_2 and O_2 minimizes differences in equilibration times seen at lower dosing concentrations. (c) Normalized O_2 and N_2 desorption kinetic traces collected for $Cu_{2.7}$-MFU-4*l* following dosing at variable temperatures. Oxygen desorption is more gradual than N_2 desorption, and this difference is enhanced at a lower temperature.

under dynamic conditions (see below). Interestingly, predicted N_2/Ar and O_2/Ar selectivities suggest that $Cu_{2.7}$-MFU-4*l* may also be appropriate for removing N_2 and O_2 impurities in Ar purification (Figure S12).

In addition to a high capacity and selectivity for O_2 over the other components of air, an ideal O_2-selective adsorbent would exhibit robustness to humidity and a low affinity for water, thus potentially enabling air separations without the need for pretreatment to remove moisture. The Cu^I-MFU-4*l* framework was previously reported to be air-stable, and in our hands, a sample of $Cu_{2.7}$-MFU-4*l* was found to be robust to ambient air for 3 months, based on powder X-ray diffraction analysis (Figure S40). Furthermore, DRIFTS data collected for a sample of $Cu_{2.7}$-MFU-4*l* exposed to the atmosphere at 300 K revealed the stable coordination of both N_2 and O_2 over the course of at least 10 h without any additional changes in color (Figure S36). A water isotherm collected for $Cu_{2.7}$-MFU-4*l* at 298 K at relative humidity levels ranging from 2 to 80% revealed that the material has a low affinity for water (Figure S14), in contrast to the parent framework MFU-4*l*.[49] Consistent with this result, DFT calculations predict an electronic energy of −27 kJ/mol for water adsorption at the copper(I) sites in the framework, indicating a weaker metal−adsorbate interaction compared to the binding of O_2 or N_2 to the exposed copper(I) site.[50]

Additionally, while the O_2, N_2, and Ar adsorption isotherms of $Cu_{2.7}$-MFU-4*l* were completed within several hours, the completion of the water adsorption isotherm required approximately 50 h, indicative of sluggish water uptake kinetics. A small amount of hysteresis upon water desorption may be due to the formation of water clusters within the pores.[49,51] Powder X-ray diffraction analysis of $Cu_{2.7}$-MFU-4*l* following water adsorption/desorption isotherms collected at 298 and 308 K revealed that the material remains crystalline (Figure S38). These observations contrast the behavior of $Cu_{2.2}$-MFU-4*l*, which exhibits substantial loss of crystallinity following water adsorption/desorption isotherms at 298 K. Finally, to probe the stability of $Cu_{2.7}$-MFU-4*l* at 100% relative humidity under relevant conditions, we dosed a sample of the material with air presaturated with water for 30 min at 25 °C. The material was then reactivated (see Section S1.16 of the Supporting Information for details) and powder X-ray diffraction and O_2 adsorption and desorption data were collected. The framework retained crystallinity, and the isothermal adsorption data are indistinguishable from that collected for the pristine material (see Figures S41 and S10, respectively), indicating excellent material stability.

Adsorption/Desorption Cycling Performance under Dry Air. To gain initial insight into the cycling stability of $Cu_{2.7}$-MFU-4*l* under more realistic O_2 capture conditions, we performed thermogravimetric analysis adsorption/desorption cycling experiments by exposing a sample of the material to flowing dry air (10 min at 30 °C), followed by desorption under a simulated vacuum (Ar purge, 10 min at 30 °C). Remarkably, the material retained >99.9% of its total capacity over the course of 40 cycles, although we note that the weight change measured under these conditions reflects both adsorbed O_2 and N_2 (Figure S18). Adsorption/desorption cycling data were also collected under simulated temperature swing conditions by exposing the material to dry air (5 min at 30 °C), followed by desorption under an O_2 purge at higher temperature (30 s at 100 °C). Under these conditions, incomplete desorption was observed, and a capacity of ∼95% (O_2 and N_2) was retained over 40 cycles (Figure S19). The slightly lower capacity relative to that measured under simulated pressure swing conditions is attributed to the highly oxidizing conditions used for desorption.

Kinetics Measurements. Adsorption and desorption kinetics are also critical factors to consider in assessing the utility of a candidate adsorbent. We investigated the kinetics of O_2 and N_2 adsorption and desorption in $Cu_{2.7}$-MFU-4*l* at temperatures of 288, 298, and 308 K after dosing with initial quantities of each adsorbate (0.5, 1.0, 5.0, or 10.0 mmol/g) corresponding to equilibrated pressures ranging from approximately 3 to 330 mbar (see Table S5; these pressures reflecting the steep region of the single-component isotherms for each gas). Adsorption of O_2 and N_2 occurred rapidly in $Cu_{2.7}$-MFU-4*l*, with pressure equilibration occurring within approximately 50 s or less in both cases and for all temperatures and dosing conditions (Figure S20). For both gases, the rate of adsorption increased with an increase in temperature, although this effect is more pronounced for N_2 (Figure 5a). At the lowest two dosing concentrations and all three temperatures, N_2 uptake in $Cu_{2.7}$-MFU-4*l* equilibrated more rapidly than that in O_2 (∼20 *versus* 50 s). This difference was minimized at the highest two dosing concentrations of 5.0 and 10.0 mmol/g (Figures 5b, S22, and S23), and the saturation times for both gases appeared to approach the diffusion-controlled time scales measured for Ar adsorption kinetics (∼20 s, see Figure S21).

https://doi.org/10.1021/jacs.3c10753
J. Am. Chem. Soc. 2024, 146, 3160−3170

The adsorption data collected following dosing with 1.0 mmol/g of O_2 or N_2 could be satisfactorily fit ($R^2 > 0.99$) with a pseudo-first order rate law model using the Lagergren equation.[52] Activation energies calculated using the Arrhenius equation are similar for O_2 adsorption [E_a = 10(1) kJ/mol] and N_2 adsorption [E_a = 12(1) kJ/mol] (Table S6 and Figure S26). Identical activation barriers were calculated using data collected under the most dilute dosing conditions (0.5 mmol/g; see Figure S27). Diffusion time constants calculated from the kinetics data (see the Supporting Information for details) indicate that diffusion of N_2 is more rapid than O_2, which we attribute to a weaker N_2 binding within the framework (Table S7 and Figure S28).[53] The relatively large diffusion time constants are indicative of rapid diffusion kinetics facilitated by large framework pores.

Following adsorption analysis, variable-temperature O_2 and N_2 desorption kinetics data were collected under reduced pressure (Figures 5c, S24, and S25), which revealed that O_2 desorption from the material is more sluggish than N_2 desorption. For example, after dosing with 1.0 mmol/g of each adsorbate at 298 K, half-life ($t_{1/2}$) values extracted for O_2 and N_2 desorption were 161 and 16 s, respectively (Figure 5c), and this difference becomes even more pronounced upon lowering the temperature to 288 K ($t_{1/2}$ values of 260 and 53 s, respectively; see Figures S24 and S25). The desorption curves for both gases were fit using a pseudo-first order rate law, and the resulting data were used to calculate activation barriers for O_2 and N_2 desorption of E_a = 45(1) and 30(1) kJ/mol, respectively (Figure S26 and Table S6). Importantly, although the kinetics of O_2 and N_2 adsorption in $Cu_{2.7}$-MFU-4*l* are similar and both gases are expected to be adsorb under conditions relevant to air capture, these results suggest that it may be possible to tailor the desorption conditions to isolate high-purity O_2.

Breakthrough Analysis. Breakthrough measurements were conducted at 25 °C using pelletized $Cu_{2.7}$-MFU-4*l* and compressed air inlet streams (2 mL/min) with varying levels of humidity to assess the selectivity of $Cu_{2.7}$-MFU-4*l* for O_2 and N_2 under more realistic conditions (see Section S1.13 of the Supporting Information for details). We note that negligible uptake of CO_2 in anticipated under these conditions based on single-component CO_2 adsorption data collected for isotherm $Cu_{2.7}$-MFU-4*l* at 25 °C (Figure S11). When the material was exposed to dry air, a sharp breakthrough of N_2 occurred after 10 min, followed by breakthrough of O_2 after 25 min. This result highlights the selective nature of the binding of O_2 in $Cu_{2.7}$-MFU-4*l* under these conditions (Figure 6a). Additionally, while not the focus of this work, the separation of the N_2 and O_2 breakthrough products under these conditions suggests that $Cu_{2.7}$-MFU-4*l* may also be a viable adsorbent for purifying N_2 from air, although we note that in this case pretreatment of the air, or post-treatment of the recovered N_2, may be needed to separate other trace air contaminants, depending on the intended use and required N_2 purity. Following breakthrough of N_2 from the column, the normalized outlet flow rate (F/F_0) for N_2 temporarily exceeded the inlet flow rate, indicative of roll-up[54] from displacement of bound N_2 by O_2 due to competitive adsorption at the same bind sites. After this initial breakthrough run, the material was regenerated with heating at 150 °C under a He purge (until O_2, N_2, and H_2O were no longer detected in the outlet stream), completing the first breakthrough "cycle". The material was then cooled to ambient temperature, and two more adsorption/desorption cycles were performed under the same conditions. The breakthrough times and capacities for O_2 and N_2 did not change over the course of these three cycles (Figures 6a and S51 and Table S12).

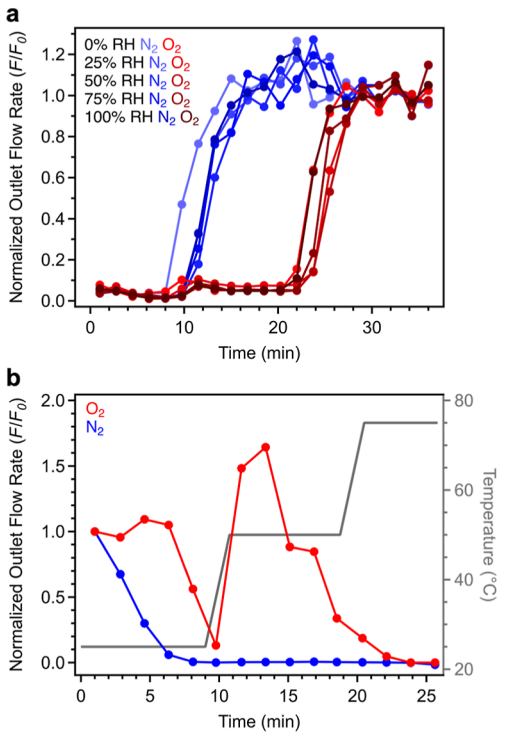

Figure 6. (a) Breakthrough profiles collected for $Cu_{2.7}$-MFU-4*l* exposed to compressed air streams with the indicated humidity levels. Sharp breakthrough of N_2 occurs before O_2, highlighting the selectivity of the framework for O_2 over N_2. Symbols correspond to averages of data from triplicate runs, and solid lines are guides for the eye (see Figures S51–S55 for individual data sets and Table S12). Small quantities of O_2 detected after 10 min before breakthrough are attributed to displacement of a small amount of O_2 by N_2. A small amount of both gases detected above the baseline at $t = 0$ is attributed to trace air present within the connection between the breakthrough column and the gas chromatograph that remains after flushing the system prior to the start of the measurement (see Section S1.13 of the Supporting Information and Figure S62 for details). (b) Oxygen and N_2 desorption breakthrough profiles for $Cu_{2.7}$-MFU-4*l*. Nitrogen was desorbed first by purging the material with He gas at 25 °C, and O_2 was subsequently desorbed under He gas at 50 °C. The O_2 and N_2 concentrations were quantified using gas chromatography, which led to a relatively low signal-to-noise ratio.

Using the same sample, three breakthrough cycles were subsequently carried out in succession, involving adsorption of compressed air streams with relative humidity levels of 25, 50, 75, and 100% and regeneration with heating at 150 °C under He (Figures S52–S55). There was no significant change in the measured breakthrough times for O_2 over the course of the 15 adsorption runs (Figure 6a), and there was no apparent change in the corresponding material capacity (Figures S56 and S57 and Table S12). Indeed, the average O_2 capacity from triplicate measurements under dry conditions was the same as that measured at the highest humidity (Figure S56 and Table S12), indicating that water neither hinders the material performance nor competes with O_2 for binding at the copper(I) sites. Finally, after the third breakthrough run at 100% relative humidity, two additional breakthrough cycles at the same relative humidity were performed with more mild regeneration under flowing He at only 50 °C (Figure S55). Although some

https://doi.org/10.1021/jacs.3c10753
J. Am. Chem. Soc. 2024, 146, 3160−3170

water remains adsorbed in the material following desorption under these conditions (Figure S60), there was no apparent change in the material capacity.

The O_2 and N_2 capacities determined from averaging over all 17 breakthrough runs are 1.2 and 1.7 mmol/g, respectively. These capacities differ slightly from those determined from single-component isotherm data, namely, 1.5 and 1.3 mmol/g, respectively. A lower O_2 capacity from breakthrough analysis is consistent with competition between O_2 and N_2 binding in the material, highlighting the fact that single-component adsorption data may not accurately reflect the adsorption behavior of a MOF when exposed to a mixed-gas stream. Interestingly, the N_2 capacities determined from the humid breakthrough data are overall higher than the single-component adsorption capacity. This phenomenon is currently not understood, and while the capacity values should be interpreted with caution in the absence of statistical errors, this result may indicate that the presence of humidity enhances N_2 uptake in $Cu_{2.7}$-MFU-4*l*. Importantly, the breakthrough data reveal that the framework retains selectivity for O_2 over N_2 when exposed to air streams with varying humidity levels, and also that there is an enhancement in the quantity of O_2 in the adsorbed phase in $Cu_{2.7}$-MFU-4*l* relative to ambient air.

Finally, we sought to exploit the differences in N_2 and O_2 desorption kinetics discussed above and identify conditions, under which it would be possible to separately isolate adsorbed N_2 and O_2. We found that it is indeed possible to desorb the majority of the bound N_2 from the material at 25 °C under simulated vacuum with a He purge, after which point high-purity O_2 can be isolated from the material (containing <0.5% N_2 based on analysis of the stream composition using gas chromatography) by ramping the temperature to 50 °C (Figure 6b). Desorption of both N_2 and O_2 could also be conducted entirely at 25 °C, albeit with relatively sluggish kinetics for complete O_2 desorption, indicating a trade-off between desorption rates and thermal input for regeneration (Figure S59).

CONCLUSIONS

We have optimized the synthesis of the well-known metal−organic framework Cu^I-MFU-4*l* and studied its O_2 binding properties under various conditions relevant to O_2 capture from air in the presence of water vapor. Spectroscopic, magnetic, and computational analyses revealed that the copper(I) sites bind to O_2 *via* electron transfer to form copper(II)−superoxo species. Interestingly, the superoxo moieties bind in both side- and end-on modes at the copper(II) sites, and these modes are in equilibrium over a range of temperatures. Breakthrough cycling experiments indicate the material is stable to extended cycling under dry and humid air streams and reversibly captures O_2 from ambient air in the presence of water. While both O_2 and N_2 rapidly adsorb in the material under these conditions, the activation barrier for O_2 desorption is higher than that for N_2 desorption, and this feature can be exploited to access high-purity O_2 (>99%) after initial N_2 desorption. Breakthrough analyses further indicate that the O_2 capacity of the material is unaffected by the presence of humidity, suggesting coadsorbed water does not bind to the exposed Cu^I sites. These results highlight the advantages of using soft copper(I) sites in MOFs for selective O_2 capture in the presence of water. Further, while high adsorption selectivity for O_2 over N_2 has traditionally been sought in candidate MOFs for O_2-selective air separations, our results reveal that differences in the desorption kinetics can be used to access high purity O_2 even when adsorption behavior suggests relatively low selectivity for O_2. This discovery suggests that it may be worthwhile to reinvestigate existing materials that have been overlooked based on preliminary analysis of their single-component O_2 and N_2 adsorption behavior. Research is ongoing in our laboratory to further advance Cu^I-MFU-4*l* for practical air separations, including the scaleup of the materials developed here, the impact of trace air contaminants on long-term stability, and the study of hydrophobic polymer[55] coatings to minimize water uptake.

ASSOCIATED CONTENT

Supporting Information

The Supporting Information is available free of charge at https://pubs.acs.org/doi/10.1021/jacs.3c10753.

Additional synthesis and characterization details, adsorption, kinetics, breakthrough, and computational data (PDF)

(CIF)

AUTHOR INFORMATION

Corresponding Author

Jeffrey R. Long − *Institute for Decarbonization Materials, University of California, Berkeley, Berkeley, California 94720, United States; Department of Chemistry and Department of Chemical and Biomolecular Engineering, University of California, Berkeley, Berkeley, California 94720, United States; Materials Sciences Division, Lawrence Berkeley National Laboratory, Berkeley, California 94720, United States;* orcid.org/0000-0002-5324-1321; Email: jrlong@berkeley.edu

Authors

Kurtis M. Carsch − *Institute for Decarbonization Materials, University of California, Berkeley, Berkeley, California 94720, United States; Department of Chemistry, University of California, Berkeley, Berkeley, California 94720, United States;* orcid.org/0000-0003-4432-7518

Adrian J. Huang − *Institute for Decarbonization Materials, University of California, Berkeley, Berkeley, California 94720, United States; Department of Chemistry, University of California, Berkeley, Berkeley, California 94720, United States*

Matthew N. Dods − *Institute for Decarbonization Materials, University of California, Berkeley, Berkeley, California 94720, United States; Department of Chemical and Biomolecular Engineering, University of California, Berkeley, Berkeley, California 94720, United States*

Surya T. Parker − *Department of Chemical and Biomolecular Engineering, University of California, Berkeley, Berkeley, California 94720, United States;* orcid.org/0000-0001-8534-8361

Rachel C. Rohde − *Institute for Decarbonization Materials, University of California, Berkeley, Berkeley, California 94720, United States; Department of Chemistry, University of California, Berkeley, Berkeley, California 94720, United States*

Henry Z. H. Jiang − *Institute for Decarbonization Materials, University of California, Berkeley, Berkeley, California 94720, United States; Department of Chemistry, University of*

California, Berkeley, Berkeley, California 94720, United States; Materials Sciences Division, Lawrence Berkeley National Laboratory, Berkeley, California 94720, United States

Yuto Yabuuchi − *Institute for Decarbonization Materials, University of California, Berkeley, Berkeley, California 94720, United States; Department of Chemistry, University of California, Berkeley, Berkeley, California 94720, United States; Materials Sciences Division, Lawrence Berkeley National Laboratory, Berkeley, California 94720, United States;* orcid.org/0000-0003-3034-558X

Sarah L. Karstens − *Institute for Decarbonization Materials, University of California, Berkeley, Berkeley, California 94720, United States; Department of Chemistry, University of California, Berkeley, Berkeley, California 94720, United States*

Hyunchul Kwon − *Institute for Decarbonization Materials, University of California, Berkeley, Berkeley, California 94720, United States; Department of Chemistry, University of California, Berkeley, Berkeley, California 94720, United States*

Romit Chakraborty − *Department of Chemistry, University of California, Berkeley, Berkeley, California 94720, United States; Materials Sciences Division, Lawrence Berkeley National Laboratory, Berkeley, California 94720, United States*

Karen C. Bustillo − *National Center for Electron Microscopy, Molecular Foundry, Lawrence Berkeley National Laboratory, Berkeley, California 94720, United States;* orcid.org/0000-0002-2096-6078

Katie R. Meihaus − *Institute for Decarbonization Materials, University of California, Berkeley, Berkeley, California 94720, United States; Department of Chemistry, University of California, Berkeley, Berkeley, California 94720, United States*

Hiroyasu Furukawa − *Institute for Decarbonization Materials, University of California, Berkeley, Berkeley, California 94720, United States; Department of Chemistry, University of California, Berkeley, Berkeley, California 94720, United States; Materials Sciences Division, Lawrence Berkeley National Laboratory, Berkeley, California 94720, United States;* orcid.org/0000-0002-6082-1738

Andrew M. Minor − *National Center for Electron Microscopy, Molecular Foundry, Lawrence Berkeley National Laboratory, Berkeley, California 94720, United States; Department of Materials Science and Engineering, University of California, Berkeley, Berkeley, California 94720, United States;* orcid.org/0000-0003-3606-8309

Martin Head-Gordon − *Institute for Decarbonization Materials, University of California, Berkeley, Berkeley, California 94720, United States; Department of Chemistry, University of California, Berkeley, Berkeley, California 94720, United States; Materials Sciences Division, Lawrence Berkeley National Laboratory, Berkeley, California 94720, United States;* orcid.org/0000-0002-4309-6669

Complete contact information is available at: https://pubs.acs.org/10.1021/jacs.3c10753

Author Contributions

The manuscript was written through contributions of all authors. All authors have given approval to the final version of the manuscript.

Notes

The authors declare the following competing financial interest(s): The University of California, Berkeley, has applied for a patent on some of the technology discussed here for the separation of oxygen from air, on which K.M.C. and J.R.L. are listed as co-inventors.

■ ACKNOWLEDGMENTS

Gas adsorption analyses, spectroscopic measurements, and electronic structure calculations were supported by the U.S. Department of Energy, Office of Basic Energy Sciences, Separation Science in the Chemical Sciences, Geosciences, and Biosciences Division, under award number DE-SC0019992. The synthesis of materials was supported by the Hydrogen Materials—Advanced Research Consortium (HyMARC), established as part of the Energy Materials Network under the U.S. Department of Energy, Hydrogen and Fuel Cell Technologies Office, under contract no. DE-AC02-05CH11231. K.M.C. is supported by an Arnold O. Beckman postdoctoral fellowship. This research used resources of the National Energy Research Scientific Computing Center (NERSC), a U.S. Department of Energy Office of Science User Facility located at Lawrence Berkeley National Laboratory, operated under contract no. DE-AC02-05CH11231 using NERSC award BES-ERCAP-0023680. Synchrotron powder X-ray diffraction data were collected on Beamline 17-BNM-B at the Advanced Photon Source, a DOE Office of Science User Facility, operated by Argonne National Laboratory under contract DE-AC02-06CH1135. Electron microscopy was supported by the U.S. Department of Energy, Office of Science, Basic Energy Sciences, Materials Sciences and Engineering Division under Contract No. DE-AC02-05-CH11231 within the Electron Microscopy of Soft Matter Program (KC11BN) and carried out at the Molecular Foundry, which is supported by the Office of Science, Office of Basic Energy Sciences, of the U.S. Department of Energy under Contract No. DE-AC02-05CH1123. We thank Dr. T. David Harris (UC Berkeley) for helpful discussions and A. Yakovenko, W. Xu, B. Trump (NIST), and M. V. Paley (UC Berkeley) for assistance in collecting powder X-ray diffraction data.

■ REFERENCES

(1) Huang, J.; Huang, J.; Liu, X.; Li, C.; Ding, L.; Yu, H. The Global Oxygen Budget and Its Future Projection. *Sci. Bull.* **2018**, *63*, 1180−1186.

(2) Duke, T.; Graham, S. M.; Cherian, M. N.; Ginsburg, A. S.; English, M.; Howie, S.; Peel, D.; Enarson, P. M.; Wilson, I. H.; Were, W. Oxygen Is an Essential Medicine: A Call for International Action. *Int. J. Tuberc. Lung Dis.* **2010**, *14*, 1362−1368.

(3) Kirschner, M. J.; Alekseev, A.; Dowy, S.; Grahl, M.; Jansson, L.; Keil, P.; Lauermann, G.; Meilinger, M.; Schmehl, W.; Weckler, H.; Windmeier, C. Oxygen. In *Ullmann's Encyclopedia of Industrial Chemistry*; Wiley-VCH Verlag GmbH & Co. KGaA, 2017; pp 1−32.

(4) Jaramillo, D. E.; Jaffe, A.; Snyder, B. E. R.; Smith, A.; Taw, E.; Rohde, R. C.; Dods, M. N.; DeSnoo, W.; Meihaus, K. R.; Harris, T. D.; Neaton, J. B.; Long, J. R. Metal−Organic Frameworks as O_2-Selective Adsorbents for Air Separations. *Chem. Sci.* **2022**, *13*, 10216−10237.

(5) Gaffney, T. R. Porous Solids for Air Separation. *Curr. Opin. Solid State Mater. Sci.* **1996**, *1*, 69−75.

(6) Chen, D.; Martell, A. Dioxygen Affinities of Synthetic Cobalt Schiff Base Complexes. *Inorg. Chem.* **1987**, *26*, 1026−1030.

(7) Bloch, E. D.; Murray, L. J.; Queen, W. L.; Chavan, S.; Maximoff, S. N.; Bigi, J. P.; Krishna, R.; Peterson, V. K.; Grandjean, F.; Long, G.

J.; Smit, B.; Bordiga, S.; Brown, C. M.; Long, J. R. Selective Binding of O_2 over N_2 in a Redox-Active Metal−Organic Framework with Open Iron(II) Coordination Sites. *J. Am. Chem. Soc.* **2011**, *133*, 14814−14822.
(8) Anderson, J. S.; Gallagher, A. T.; Mason, J. A.; Harris, T. D. A Five-Coordinate Heme Dioxygen Adduct Isolated within a Metal-Organic Framework. *J. Am. Chem. Soc.* **2014**, *136*, 16489−16492.
(9) Reed, D. A.; Xiao, D. J.; Jiang, H. Z.; Chakarawet, K.; Oktawiec, J.; Long, J. R. Biomimetic O_2 Adsorption in an Iron Metal-Organic Framework for Air Separation. *Chem. Sci.* **2020**, *11*, 1698−1702.
(10) Gallagher, A. T.; Kelty, M. L.; Park, J. G.; Anderson, J. S.; Mason, J. A.; Walsh, J. P. S.; Collins, S. L.; Harris, T. D. Dioxygen Binding at a Four-Coordinate Cobaltous Porphyrin Site in a Metal-Organic Framework: Structural, EPR, and O_2 Adsorption Analysis. *Inorg. Chem. Front.* **2016**, *3*, 536−540.
(11) Xiao, D. J.; Gonzalez, M. I.; Darago, L. E.; Vogiatzis, K. D.; Haldoupis, E.; Gagliardi, L.; Long, J. R. Selective, Tunable O_2 Binding in Cobalt(II)-Triazolate/Pyrazolate Metal-Organic Frameworks. *J. Am. Chem. Soc.* **2016**, *138*, 7161−7170.
(12) Rosen, A. S.; Mian, M. R.; Islamoglu, T.; Chen, H.; Farha, O. K.; Notestein, J. M.; Snurr, R. Q. Tuning the Redox Activity of Metal-Organic Frameworks for Enhanced, Selective O_2 Binding: Design Rules and Ambient Temperature O_2 Chemisorption in a Cobalt-Triazolate Framework. *J. Am. Chem. Soc.* **2020**, *142*, 4317−4328.
(13) Oktawiec, J.; Jiang, H. Z. H.; Vitillo, J. G.; Reed, D. A.; Darago, L. E.; Trump, B. A.; Bernales, V.; Li, H.; Colwell, K. A.; Furukawa, H.; Brown, C. M.; Gagliardi, L.; Long, J. R. Negative Cooperativity upon Hydrogen Bond-Stabilized O_2 Adsorption in a Redox-Active Metal-Organic Framework. *Nat. Commun.* **2020**, *11*, 3087.
(14) Murray, L. J.; Dinca, M.; Yano, J.; Chavan, S.; Bordiga, S.; Brown, C. M.; Long, J. R. Highly-Selective and Reversible O_2 Binding in Cr_3(1,3,5-Benzenetricarboxylate)$_2$. *J. Am. Chem. Soc.* **2010**, *132*, 7856−7857.
(15) Bloch, E. D.; Queen, W. L.; Hudson, M. R.; Mason, J. A.; Xiao, D. J.; Murray, L. J.; Flacau, R.; Brown, C. M.; Long, J. R. Hydrogen Storage and Selective, Reversible O_2 Adsorption in a Metal-Organic Framework with Open Chromium(II) Sites. *Angew. Chem. Int. Ed.* **2016**, *55*, 8605−8609.
(16) Sutton, A. L.; Melag, L.; Sadiq, M. M.; Hill, M. R. Capture, Storage, and Release of Oxygen by Metal-Organic Frameworks (MOFs). *Angew. Chem. Int. Ed.* **2022**, *61*, No. e202208305.
(17) Rege, S. U.; T. Yang, R.; Buzanowski, M. A. Sorbents for Air Prepurification in Air Separation. *Chem. Eng. Sci.* **2000**, *55*, 4827−4838.
(18) Young, A. F.; Villardi, H. G. D.; Araujo, L. S.; Raptopoulos, L. S. C.; Dutra, M. S. Detailed Design and Economic Evaluation of a Cryogenic Air Separation Unit with Recent Literature Solutions. *Ind. Eng. Chem. Res.* **2021**, *60*, 14830−14844.
(19) Rege, S. U.; Yang, R. T.; Qian, K.; Buzanowski, M. A. Air-Prepurification by Pressure Swing Adsorption Using Single/Layered Beds. *Chem. Eng. Sci.* **2001**, *56*, 2745−2759.
(20) Mullangi, D.; Evans, H. A.; Yildirim, T.; Wang, Y.; Deng, Z.; Zhang, Z.; Mai, T. T.; Wei, F.; Wang, J.; Hight Walker, A. R.; Brown, C. M.; Zhao, D.; Canepa, P.; Cheetham, A. K. Noncryogenic Air Separation Using Aluminum Formate $Al(HCOO)_3$ (ALF). *J. Am. Chem. Soc.* **2023**, *145*, 9850−9856.
(21) Jaffe, A.; Ziebel, M. E.; Halat, D. M.; Biggins, N.; Murphy, R. A.; Chakarawet, K.; Reimer, J. A.; Long, J. R. Selective, High-Temperature O_2 Adsorption in Chemically Reduced, Redox-Active Iron-Pyrazolate Metal-Organic Frameworks. *J. Am. Chem. Soc.* **2020**, *142*, 14627−14637.
(22) Lee, K.; Howe, J. D.; Lin, L.-C.; Smit, B.; Neaton, J. B. Small-Molecule Adsorption in Open-Site Metal-Organic Frameworks: A Systematic Density Functional Theory Study for Rational Design. *Chem. Mater.* **2015**, *27*, 668−678.
(23) Liu, X.; Wang, X.; Kapteijn, F. Water and Metal-Organic Frameworks: From Interaction toward Utilization. *Chem. Rev.* **2020**, *120*, 8303−8377.
(24) Denysenko, D.; Grzywa, M.; Jelic, J.; Reuter, K.; Volkmer, D. Scorpionate-Type Coordination in MFU-4*l* Metal-Organic Frameworks: Small-Molecule Binding and Activation upon the Thermally Activated Formation of Open Metal Sites. *Angew. Chem., Int. Ed.* **2014**, *53*, 5832−5836.
(25) Naskar, J. P.; Hati, S.; Datta, D.; Tocher, D. A. First Example of a Copper(I)-Water Bond. Synthesis and Structure of Polymeric Poly-μ-2,3-Diphenylquinoxaline-(Aqua)Copper(I) Cation. *Chem. Commun.* **1997**, *14*, 1319−1320.
(26) Barnett, B. R.; Evans, H. A.; Su, G. M.; Jiang, H. Z. H.; Chakraborty, R.; Banyeretse, D.; Hartman, T. J.; Martinez, M. B.; Trump, B. A.; Tarver, J. D.; Dods, M. N.; Funke, L. M.; Börgel, J.; Reimer, J. A.; Drisdell, W. S.; Hurst, K. E.; Gennett, T.; FitzGerald, S. A.; Brown, C. M.; Head-Gordon, M.; Long, J. R. Observation of an Intermediate to H_2 Binding in a Metal-Organic Framework. *J. Am. Chem. Soc.* **2021**, *143*, 14884−14894.
(27) Su, G. M.; Wang, H.; Barnett, B. R.; Long, J. R.; Prendergast, D.; Drisdell, W. S. Backbonding Contributions to Small Molecule Chemisorption in a Metal-Organic Framework with Open Copper(I) Centers. *Chem. Sci.* **2021**, *12*, 2156−2164.
(28) Mohamed, M. H.; Yang, Y.; Li, L.; Zhang, S.; Ruffley, J. P.; Jarvi, A. G.; Saxena, S.; Veser, G.; Johnson, J. K.; Rosi, N. L. Designing Open Metal Sites in Metal-Organic Frameworks for Paraffin/Olefin Separations. *J. Am. Chem. Soc.* **2019**, *141*, 13003−13007.
(29) Li, L.; Yang, Y.; Mohamed, M. H.; Zhang, S.; Veser, G.; Rosi, N. L.; Johnson, J. K. Fundamental Insights into the Reactivity and Utilization of Open Metal Sites in Cu(I)-MFU-4l. *Organometallics* **2019**, *38*, 3453−3459.
(30) We strongly encourage future reports on the synthesis of Cu(I)-MFU-4*l* to benchmark 77 K H_2 isotherm capacity at 1 mbar.
(31) Mian, M. R.; Chen, H.; Cao, R.; Kirlikovali, K. O.; Snurr, R. Q.; Islamoglu, T.; Farha, O. K. Insights into Catalytic Hydrolysis of Organophosphonates at M-OH Sites of Azolate-Based Metal Organic Frameworks. *J. Am. Chem. Soc.* **2021**, *143*, 9893−9900.
(32) Denysenko, D.; Jelic, J.; Reuter, K.; Volkmer, D. Postsynthetic Metal and Ligand Exchange in MFU-4l: A Screening Approach toward Functional Metal-Organic Frameworks Comprising Single-Site Active Centers. *Chem. Eur. J.* **2015**, *21* (22), 8188−8199.
(33) Evans, A. D.; Cummings, M. S.; Luebke, R.; Brown, M. S.; Favero, S.; Attfield, M. P.; Siperstein, F.; Fairen-Jimenez, D.; Hellgardt, K.; Purves, R.; Law, D.; Petit, C. Screening Metal-Organic Frameworks for Dynamic CO/N_2 Separation Using Complementary Adsorption Measurement Techniques. *Ind. Eng. Chem. Res.* **2019**, *58*, 18336−18344.
(34) Wright, A. M.; Sun, C.; Dincă, M. Thermal Cycling of a MOF-Based NO Disproportionation Catalyst. *J. Am. Chem. Soc.* **2021**, *143* (2), 681−686.
(35) Hou, K.; Börgel, J.; Jiang, H. Z. H.; SantaLucia, D. J.; Kwon, H.; Zhuang, H.; Chakarawet, K.; Rohde, R. C.; Taylor, J. W.; Dun, C.; Paley, M. V.; Turkiewicz, A. B.; Park, J. G.; Mao, H.; Zhu, Z.; Alp, E. E.; Zhao, J.; Hu, M. Y.; Lavina, B.; Peredkov, S.; Lv, X.; Oktawiec, J.; Meihaus, K. R.; Pantazis, D. A.; Vandone, M.; Colombo, V.; Bill, E.; Urban, J. J.; Britt, R. D.; Grandjean, F.; Long, G. J.; DeBeer, S.; Neese, F.; Reimer, J. A.; Long, J. R. Reactive High-Spin Iron(IV)-Oxo Sites through Dioxygen Activation in a Metal-Organic Framework. *Science* **2023**, *382*, 547−553.
(36) Elwell, C. E.; Gagnon, N. L.; Neisen, B. D.; Dhar, D.; Spaeth, A. D.; Yee, G. M.; Tolman, W. B. Copper-Oxygen Complexes Revisited: Structures, Spectroscopy, and Reactivity. *Chem. Rev.* **2017**, *117*, 2059−2107.
(37) Tomson, N. C.; Williams, K. D.; Dai, X.; Sproules, S.; DeBeer, S.; Warren, T. H.; Wieghardt, K. Re-Evaluating the Cu K Pre-Edge XAS Transition in Complexes with Covalent Metal-Ligand Interactions. *Chem. Sci.* **2015**, *6*, 2474−2487.
(38) Ginsbach, J. W.; Peterson, R. L.; Cowley, R. E.; Karlin, K. D.; Solomon, E. I. Correlation of the Electronic and Geometric Structures in Mononuclear Copper(II) Superoxide Complexes. *Inorg. Chem.* **2013**, *52*, 12872−12874.

https://doi.org/10.1021/jacs.3c10753
J. Am. Chem. Soc. 2024, 146, 3160−3170

(39) Maiti, D.; Fry, H. C.; Woertink, J. S.; Vance, M. A.; Solomon, E. I.; Karlin, K. D. A 1:1 Copper-Dioxygen Adduct Is an End-on Bound Superoxo Copper(II) Complex Which Undergoes Oxygenation Reactions with Phenols. *J. Am. Chem. Soc.* **2007**, *129*, 264−265.
(40) Donoghue, P. J.; Gupta, A. K.; Boyce, D. W.; Cramer, C. J.; Tolman, W. B. An Anionic, Tetragonal Copper(II) Superoxide Complex. *J. Am. Chem. Soc.* **2010**, *132*, 15869−15871.
(41) Würtele, C.; Gaoutchenova, E.; Harms, K.; Holthausen, M. C.; Sundermeyer, J.; Schindler, S. Crystallographic Characterization of a Synthetic 1:1 End-On Copper Dioxygen Adduct Complex. *Angew. Chem. Int. Ed.* **2006**, *45* (23), 3867−3869.
(42) Zecchina, A.; Otero Areán, C.; Turnes Palomino, G.; Geobaldo, F.; Lamberti, C.; Spoto, G.; Bordiga, S. The Vibrational Spectroscopy of H_2, N_2, CO and NO Adsorbed on the Titanosilicate Molecular Sieve ETS-10. *Phys. Chem. Chem. Phys.* **1999**, *1*, 1649−1657.
(43) Carsch, K. M.; Iliescu, A.; McGillicuddy, R. D.; Mason, J. A.; Betley, T. A. Reversible Scavenging of Dioxygen from Air by a Copper Complex. *J. Am. Chem. Soc.* **2021**, *143*, 18346−18352.
(44) Woertink, J. S.; Tian, L.; Maiti, D.; Lucas, H. R.; Himes, R. A.; Karlin, K. D.; Neese, F.; Würtele, C.; Holthausen, M. C.; Bill, E.; Sundermeyer, J.; Schindler, S.; Solomon, E. I. Spectroscopic and Computational Studies of an End-on Bound Superoxo-Cu(II) Complex: Geometric and Electronic Factors That Determine the Ground State. *Inorg. Chem.* **2010**, *49*, 9450−9459.
(45) DiMucci, I. M.; Lukens, J. T.; Chatterjee, S.; Carsch, K. M.; Titus, C. J.; Lee, S. J.; Nordlund, D.; Betley, T. A.; MacMillan, S. N.; Lancaster, K. M. The Myth of d^8 Copper(III). *J. Am. Chem. Soc.* **2019**, *141*, 18508−18520.
(46) Salem, M. M. K.; Braeuer, P.; Szombathely, M. V.; Heuchel, M.; Harting, P.; Quitzsch, K.; Jaroniec, M. Thermodynamics of High-Pressure Adsorption of Argon, Nitrogen, and Methane on Microporous Adsorbents. *Langmuir* **1998**, *14*, 3376−3389.
(47) Myers, A. L.; Prausnitz, J. M. Thermodynamics of Mixed-Gas Adsorption. *AIChE J.* **1965**, *11*, 121−127.
(48) Krishna, R.; van Baten, J. M. How Reliable Is the Ideal Adsorbed Solution Theory for the Estimation of Mixture Separation Selectivities in Microporous Crystalline Adsorbents? *ACS Omega* **2021**, *6*, 15499−15513.
(49) Wright, A. M.; Rieth, A. J.; Yang, S.; Wang, E. N.; Dincă, M. Precise Control of Pore Hydrophilicity Enabled by Post-Synthetic Cation Exchange in Metal-Organic Frameworks. *Chem. Sci.* **2018**, *9*, 3856−3859.
(50) Talbot, J. J.; Chakraborty, R.; Shen, H.; Head-Gordon, M. A Free Energy Decomposition Analysis: Insight into Binding Thermodynamics from Absolutely Localized Molecular Orbitals. *J. Phys. Chem. Lett.* **2023**, *14*, 5432−5440.
(51) Rieth, A. J.; Hunter, K. M.; Dincă, M.; Paesani, F. Hydrogen Bonding Structure of Confined Water Templated by a Metal-Organic Framework with Open Metal Sites. *Nat. Commun.* **2019**, *10*, 4771.
(52) Liu, Y.; Shen, L. From Langmuir Kinetics to First- and Second-Order Rate Equations for Adsorption. *Langmuir* **2008**, *24*, 11625−11630.
(53) Saha, D.; Deng, S. Adsorption Equilibria and Kinetics of Carbon Monoxide on Zeolite 5A, 13X, MOF-5, and MOF-177. *J. Chem. Eng. Data* **2009**, *54*, 2245−2250.
(54) Wilkins, N. S.; Rajendran, A.; Farooq, S. Dynamic Column Breakthrough Experiments for Measurement of Adsorption Equilibrium and Kinetics. *Adsorption* **2021**, *27*, 397−422.
(55) Yang, S.; Peng, L.; Sun, D. T.; Asgari, M.; Oveisi, E.; Trukhina, O.; Bulut, S.; Jamali, A.; Queen, W. L. A New Post-Synthetic Polymerization Strategy Makes Metal-Organic Frameworks More Stable. *Chem. Sci.* **2019**, *10*, 4542−4549.

https://doi.org/10.1021/jacs.3c10753
J. Am. Chem. Soc. 2024, 146, 3160−3170